AEM
Journals.ASM.org

The 60-Kilodalton Protein Encoded by *orf2* in the *cry19A* Operon of *Bacillus thuringiensis* subsp. *jegathesan* Functions Like a C-Terminal Crystallization Domain

J. Eleazar Barboza-Corona,[a] Hyun-Woo Park,[b,c] Dennis K. Bideshi,[b,c] and Brian A. Federici[b,d]

Universidad de Guanajuato Campus Irapuato-Salamanca, División Ciencias de la Vida, Departamento de Ingeniería en Alimentos, Irapuato, Guanajuato, México[a]; Department of Entomology, University of California, Riverside, Riverside, California, USA[b]; Department of Natural and Mathematical Sciences, California Baptist University, Riverside, California, USA[c]; and Interdepartmental Graduate Programs in Genetics, Genomics & Bioinformatics, and Cell, Molecular & Developmental Biology, University of California, Riverside, California, USA[d]

The *cry19A* operon of *Bacillus thuringiensis* subsp. *jegathesan* encodes two proteins, mosquitocidal Cry19A (ORF1; 75 kDa) and an ORF2 (60 kDa) of unknown function. Expression of the *cry19A* operon in an acrystalliferous strain of *B. thuringiensis* (4Q7) yielded one small crystal per cell, whereas no crystals were produced when *cry19A* or *orf2* was expressed alone. To determine the function of the ORF2 protein, different combinations of Cry19A, ORF2, and the N- or C-terminal half of Cry1C were synthesized in strain 4Q7. Stable crystalline inclusions of these fusion proteins similar in shape to those in the strain harboring the wild-type operon were observed in sporulating cells. Comparative analysis showed that ORF2 shares considerable amino acid sequence identity with the C-terminal region of large Cry proteins. Together, these results suggest that ORF2 assists in synthesis and crystallization of Cry19A by functioning like the C-terminal domain characteristic of Cry protein in the 130-kDa mass range. In addition, to determine whether overexpression of the *cry19A* operon stabilized its shape and increased Cry19A yield, it was expressed under the control of the strong chimeric *cyt1A*-p/STAB-SD promoter. Interestingly, in contrast to the expression seen with the native promoter, overexpression of the operon yielded uniform bipyramidal crystals that were 4-fold larger on average than the wild-type crystal. In bioassays using the 4th instar larvae of *Culex quinquefasciatus*, the strain producing the larger Cry19A crystal showed moderate larvicidal activity that was 4-fold (95% lethal concentration [LC_{95}] = 1.9 μg/ml) more toxic than the activity produced in the strain harboring the wild-type operon (LC_{95} = 8.2 μg/ml).

A major principle of resistance management for insecticidal proteins is the use of combinations of different proteins, especially proteins that do not share the same midgut receptors (5, 21). In this regard, endotoxins of the mosquitocidal *B. thuringiensis* subsp. *jegathesan* bacterium isolated in Malaysia (22) are of interest. This subspecies produces a parasporal body containing eight proteins (2, 17, 22, 25), and preliminary studies of one, Cry19Aa, a 75-kDa protein, have shown that it exhibits no cross-resistance to any of the Cry proteins (Cry4Aa, Cry4Ba, Cry11Aa) of *B. thuringiensis* subsp. *israelensis*, the most effective biopesticide used to control mosquito and blackfly larvae (1, 4, 7, 16, 24, 26). The gene encoding Cry19A has been cloned and sequenced and shown to occur as the first gene of an apparent two-gene operon that includes *orf2* (19). However, little is known about the molecular genetics of Cry19A synthesis and, specifically, about the role that ORF2 (60 kDa) plays in the synthesis and crystallization of Cry19A. In an initial study of the *cry19A* operon, Rosso and Delécluse (19) found that net synthesis of Cry19A was greater in the presence of intact *orf2* rather than when synthesized with a truncated version of the latter and, furthermore, that inclusions containing both Cry19A and ORF2 were more toxic than inclusions containing Cry19A alone. Regarding its function, Rosso and Delécluse (19) suggested that the *orf2* sequence has a stabilizing effect on the *cry19A* transcript, although it was considered more likely that the coded 60-kDa protein functioned as a molecular chaperone, increasing net crystal synthesis, as Cry19A degraded rapidly when cosynthesized with the truncated ORF2 protein (19).

To further investigate ORF2's role in Cry19A synthesis and to enhance cocrystallization for potential applied use, we studied the effects of expressing *cry19A* alone or together with *orf2* by using its native promoter or *cyt1A* promoters combined with the STAB-SD sequence (*cyt1A*-p/STAB-SD) (12). The chimeric *cyt1A*-p/STAB-SD expression system has been shown to significantly improve synthesis of several Cry proteins and Bin (10, 12–14), making it useful for the study of the role of ORF2 at both basic and applied levels. Here we demonstrate that by using differential expression systems, ORF2, coded in *cis* or *trans* with *cry19A*, enhances net synthesis and crystallization of Cry19A by functioning as the C-terminal crystallization domain, a function characteristic of the C-terminal domain of large (130- to 135-kDa) Cry proteins. Overexpression of the operon increased the yield of Cry19A 4-fold and, interestingly, stabilized the bipyramidal topology of the crystalline inclusion. Because ORF2 cocrystallizes with Cry19A in an apparent equimolar ratio, as determined by acrylamide gel protein profiling, it is unlikely that ORF2 is a bona fide molecular chaperone or that its coding sequence is an mRNA stabilizer, as suggested previously (19).

Received 30 August 2011 **Accepted** 2 January 2012
Published ahead of print 13 January 2012
Address correspondence to Brian A. Federici, brian.federici@ucr.edu.
J.E.B.-C. and H.-W.P. contributed equally to this article.

doi:10.1128/AEM.06750-11

TABLE 1 Primers used for PCR amplification of *cry19A* and *orf2* sequences

Primer	Sequence[a]
19A-R	5′-CGGGATCCATTCACAACCTTTTTTC TTATTTT-3′
OPN-19F	5′-AAGAAACATTATTATGGGAATAGG-3′
OPN-19R	5′-CGTTCCTCCCTTATTCCCATCATT-3′
OPN-F	5′-AACTGCAGGCATGCAACAGAACCCT AAAAAAT-3′
OPN-ORF2F	5′-TTTAAACTTACAAGTGGTGCGAAA-3′
OPN-ORF2R	5′-ATTCACAACCTTTTTTCTTATTTT-3′
OPN-R	5′-CGGGATCCATGCATAGATTCGTAAT AGTATCT-3′
ORF2-F	5′-TTT**ATG**CTTACAAGTGGTGCGAAA-3′

[a] Restriction endonuclease cleavage sites for BamHI and PstI are underlined; intact and mutated ATG codons are shown in boldface and shaded, respectively.

MATERIALS AND METHODS

Bacterial strains and plasmids. The acrystalliferous strains of *B. thuringiensis* used in this study were *B. thuringiensis* subsp. *israelensis* 4Q7 (*Bacillus* Genetic Stock Center, Columbus, OH) and *B. thuringiensis* subsp. *thuringiensis* SPL407, which contains pJEG65.5 harboring the *cry19A* operon in pHT315 (A. Delécluse, Institut Pasteur, Paris, France [19]). Cloned genes and recombinant plasmid constructs were amplified in *Escherichia coli* DH5α [*supE44*, Δ*lacU169* (F80*lacZ*ΔM15) *hsdR17 recA1 endA1 gyrA96 thi-1 relA1*]. The shuttle vectors used to transform and express the different constructs were pPG (which contained a chloramphenicol resistance gene marker), pHT315, and pSTAB, a pHT3101-derived vector containing the 660-bp *cyt1A*-p/STAB-SD strong chimeric promoter (9, 14).

Construction of recombinant plasmids. A series of recombinant plasmids were constructed for two different purposes.

(i) Analysis of the *cry19A* operon. To determine the function of ORF2 encoded by the second gene in the *cry19A* operon, pJEG65.5 in *B. thuringiensis* subsp. *thuringiensis* SPL407 was isolated using a Qiagen plasmid midi kit (Qiagen, Valencia, CA). DNA fragments containing *cry19A* and *orf2* were obtained using PCR, with pJEG65.5 as the template. Because the 3′ transcriptional termination sequence of the *cry19A* operon in pJEG65.5 was not available (19), this 1-kb region was sequenced using the M13 primers at the Core Instrument Facility, Institute for Integrative Genome Biology, University of California, Riverside, and additional primers to complete the sequence were designed based on this sequence. PCR was performed with the high-fidelity Phire Hot Start DNA Polymerase system (New England BioLabs, Ipswich, MA) in a ThermoHybaid PX2 thermocycler (Thermo Scientific, Rockford, IL) for 30 cycles. Conditions were as follows: 98°C for 30 s, 60°C for 30 s, and 72°C for 1 min and then a 2-min termination at 72°C.

The primers used to amplify different regions of the *cry19A* operon are listed in Table 1, and the plasmids constructed using the PCR products are illustrated in Fig. 1A. The primers OPN-F (containing an additional PstI site for cloning) and OPN-19R were used to amplify the 171-bp putative promoter region of the *cry19Aa1* operon. The 4,616-bp DNA fragment containing inactive *cry19A* was knocked out by modifying the start codon, and *orf2* was amplified using primers OPN-19F and OPN-R, which contained an additional BamHI site for cloning. To construct the plasmid (pHTΔ19ORF2) harboring the *cry19A* operon with *cry19A* lacking the native translation start codon, the 171-bp and 4,616-bp fragments were treated with T4 polynucleotide kinase (New England BioLabs, Beverly, MA), digested with PstI and BamHI, respectively, and ligated into pHT315. Similarly, the 2,260-bp putative promoter region plus the *cry19A* fragment that was amplified using the OPN-F and OPN-ORF2R primers and the 2,527-bp *orf2* gene that was knocked out by modifying the *orf2* start codon were amplified using primers OPN-ORF2F and OPN-R. Both

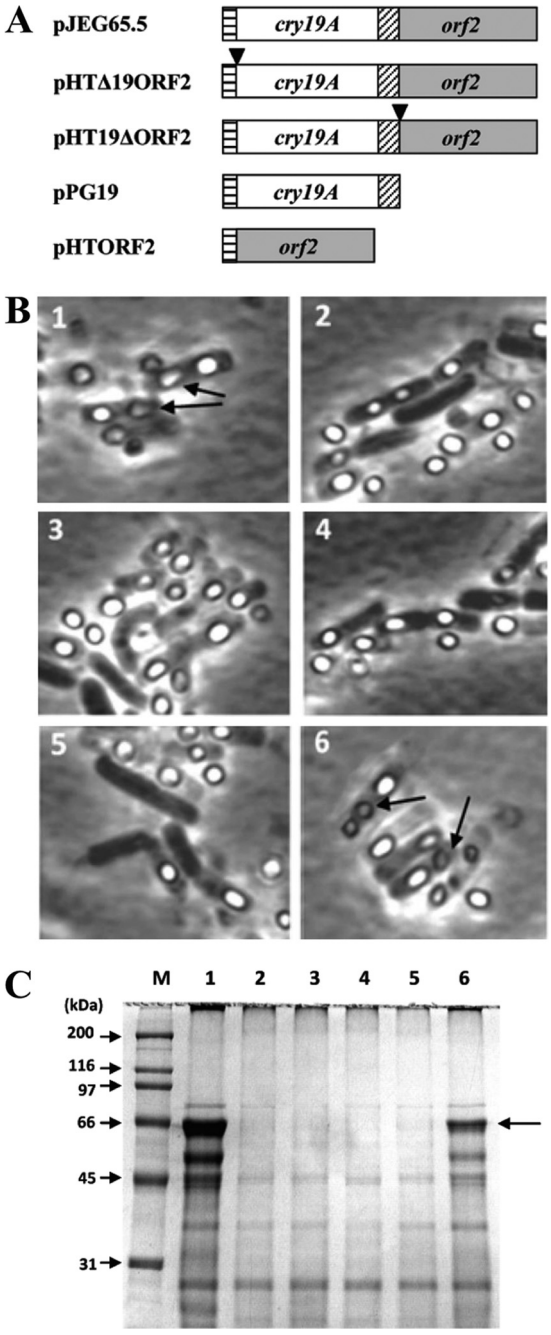

FIG 1 ORF2 is required for crystallization of Cry19A. (A) Schematic illustration of the different constructs containing *cry19A* or *orf2* or both. The translation start codons of *cry19A* and *orf2* were modified in pHTΔ19ORF2 and pHT19ΔORF2, respectively. In all constructs, expression was under the control of the wild-type promoter. (B) Phase-contrast micrographs of recombinant *B. thuringiensis* 4Q7 strains containing the plasmids illustrated in panel A. Panel 1, 4Q7/pJEG65.5; panel 2, 4Q7/pHTΔ19ORF2; panel 3, 4Q7/pHT19ΔORF2; panel 4, 4Q7/pPG19; panel 5, 4Q7/pHTORF2; panel 6, 4Q7/pPG19+pHTORF2. Arrows indicate crystals. (C) SDS-PAGE analysis of the recombinant *B. thuringiensis* 4Q7 strains containing *cry19A* or *orf2* or both. M, molecular mass marker; lane 1, 4Q7/pJEG65.5; lane 2, 4Q7/pHTΔ19ORF2; lane 3, 4Q7/pHT19ΔORF2; lane 4, 4Q7/pPG19; lane 5, 4Q7/pHTORF2; lane 6, 4Q7/pPG19+pHTORF2. Cry19A is indicated by an arrow.

TABLE 2 Primers used for amplification of different constructs of *cry19A*, *orf2*, and *cry1C*

Primer	Sequence[a]
1C-1	5′-GCGGTGAATGCCCTGTTTAC-3′
1C-2	5′-ACATGCATGCCCCCTTAGATAGATATCATAG-3′
1C-3	5′-**TCA**CTTTTGTGCTC TTTCTAAATCAGA-3′
1C-4	5′-CTTTTGTGCTC TTTCTAAATCAGA-3′
19A-1	5′-ACGCGTCGACGAATAA**GGGAGG**AACGAAGA-3′
19A-2	5′-AACTGCAGAATGTTTCCTGTGATCTTTC-3′
19A-3	5′-AACTGCAGATTCTATTCTTTTTCAAACT-3′
19A-4	5′-GTTAGTTGGGAGGAATTCGA-3′
DS-1	5′-GGAATTCTATTTTCGATTTC-3′
ORF2-1	5′-TACCATTCACAGGAAATATG-3′
ORF2-2	5′-ATGCTTACAAGTGGTGCGAAAAATATGTTA-3′

[a] The ribosome binding site and artificial stop codon (bold type) and the SphI, SalI, PstI, and EcoRI sites used for cloning (underlined) are shown.

PCR fragments were treated with T4 polynucleotide kinase (New England BioLabs, Beverly, MA), digested with PstI and BamHI, respectively, and ligated into pHT315 to generate pHT19ΔORF2, a plasmid harboring the entire *cry19A* operon with the mutated translation start codon in *orf2*. In addition, the 2,260-bp putative promoter region plus the *cry19A* fragment was amplified using the OPN-F and 19A-R primers in order to include additional PstI and BamHI sites for cloning into pPG to generate pPG19. Lastly, the 2,527-bp *orf2* fragment was amplified using the ORF2-F and OPN-R primers, and the amplicon was treated with T4 polynucleotide kinase, digested with BamHI, and ligated into pHT315 with the PstI-digested 171-bp putative promoter region described above to generate pHTORF2. All PCR products were purified using a QIAquick gel extraction kit (Qiagen, Valencia, CA), and recombinant plasmids were transformed in *E. coli* DH5α. The sequence integrity of all plasmid constructs was confirmed by restriction enzyme digestion and sequencing analysis.

(ii) Improvement of Cry19A synthesis, crystal topology, and determination of ORF2 function. DNA fragments containing *cry19A* and *cry19A-orf2* were obtained by PCR with substrate pJEG65.5 from *B. thuringiensis* subsp. *thuringiensis* SPL407. PCR was performed with an Expand Long Template PCR system (Roche Diagnostics GmbH, Germany) and a GeneAmp 2400 PCR system thermocycler (Perkin Elmer, Boston, MA) for 30 cycles. Conditions were as follows: 94°C for 1 min, 55°C for 1 min, 68°C for 4 min, and then 7 min of termination at 68°C. The forward primer, 19A-1, contained a putative ribosome binding site and an additional SalI site for cloning the PCR product into pSTAB. The reverse primers were 19A-2 (to amplify *cry19A*) and 19A-3 (to amplify the *cry19A* operon) (Table 2). Both reverse primers contained an additional PstI site. PCR products containing *cry19A* (Fig. 2A, panel a) or the *cry19A* operon (Fig. 2A, panel b) and pSTAB were purified using a QIAquick gel extraction kit (Qiagen GmbH, Germany), cut with PstI and SalI, ligated, and transformed in *E. coli*.

To determine the ORF2 function, plasmids containing the following elements were constructed as follows: *cry19A* plus *orf2* without the intergenic spacer (Fig. 3A, panel a); *cry19A* without the intergenic spacer but with the region coding for the C terminus of Cry1C (Fig. 3A, panel b); the region that codes for the Cry1C N terminus plus *orf2* with the intergenic spacer that occurs in the *cry19A* wild-type operon (Fig. 3A, panel c); and the region that codes for the Cry1C N terminus plus *orf2* without the spacer (Fig. 3A, panel d). Nucleotide sequences of *cry1C* corresponding to the N- and C-terminal halves were described previously (13). The primers used for amplification and the different constructs are shown in Table 2 and Fig. 2. DNA fragments were amplified by PCR with Vent DNA polymerase (New England BioLabs, Beverly, MA) for 30 cycles as follows: 94°C for 1 min, 55°C for 1 min, and 72°C for 3 min. For amplifying *cry1C*, pPFT1C (13) was used as the template. PCR products were purified as described above, treated with T4 polynucleotide kinase (New England BioLabs, Beverly, MA), digested with different restriction enzymes, and

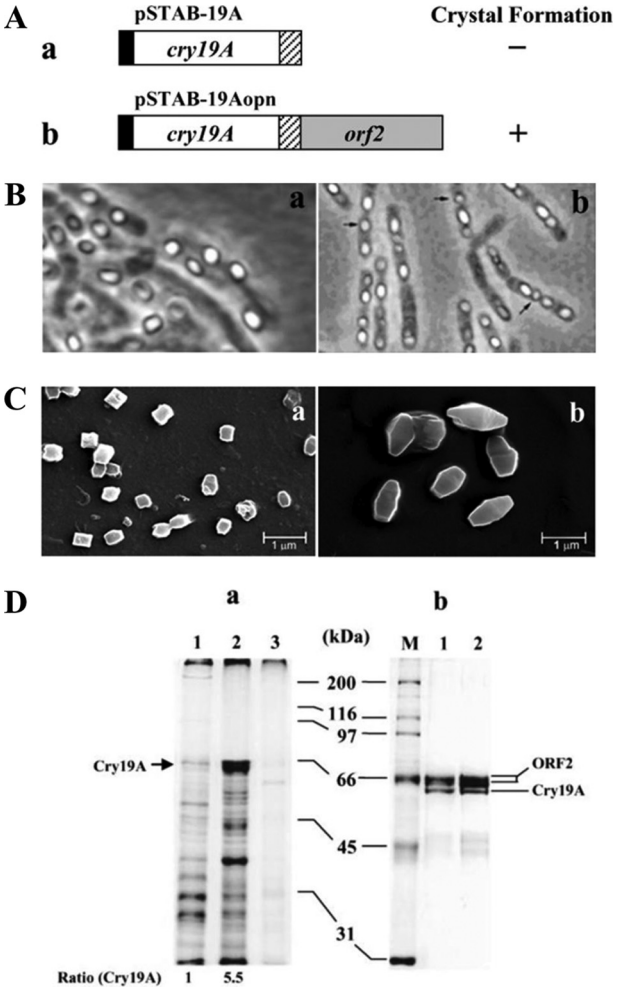

FIG 2 Overexpression of *cry19A* operon increases yield and stabilizes bipyramidal morphology of Cry19A crystalline inclusions. (A) Schematic illustration of the constructs used to synthesize Cry19A and test the function of the 60-kDa ORF2 protein. In all constructs, synthesis was under the control of the *cyt1A*-p/STAB-SD sequence. Panel a, pSTAB-19A used to synthesize Cry19A alone; panel b, pSTAB-19Aopn used to synthesize Cry19A and the 60-kDa protein together. Strains that contained or lacked crystals are indicated as (+) or (−), respectively. (B) Phase-contrast micrographs of the recombinant *B. thuringiensis* 4Q7 strains containing the plasmids illustrated in panel A. Arrows indicate crystals. Panel a, pSTAB-19A used to synthesize Cry19A alone; panel b, pSTAB-19Aopn used to synthesize Cry19A and the 60-kDa protein together. (C) Scanning electron micrographs of purified Cry19A inclusions. Panel a, inclusions produced using the wild-type *cry19A* operon (pJEG65.5) in *B. thuringiensis* strain 4Q7; panel b, inclusions produced by expressing the *cry19A* operon under the control of *cyt1A*-p/STAB-SD (pSTAB-19Aopn) in the acrystalliferous 4Q7 strain of *B. thuringiensis*. (D) Analysis of synthesis of Cry19A and the 60-kDa ORF2 protein by different *cry19A* constructs by the use of SDS-PAGE. Panel a, analysis of proteins synthesized per unit medium. Lane 1, Cry19A produced using the wild-type *cry19A* operon (pJEG65.5) in *B. thuringiensis* 4Q7; lane 2, Cry19A produced using the *cry19A* operon under the control of *cyt1A*-p/STAB-SD (pSTAB-19Aopn) in *B. thuringiensis* 4Q7; lane 3, Cry19A produced by *cyt1A*-p/STAB-SD in *B. thuringiensis* 4Q7 in the absence of the ORF2 60-kDa protein (pSTAB-19A). All lanes contained equal amounts of sporulated cell lysate. Panel b, analysis of purified Cry19A crystals. After purification, crystals were dissolved in 0.05 M Na_2C0_3 (pH 10.5), and equal amounts of protein were analyzed by SDS-PAGE. Lane M, molecular mass markers; lane 1, Cry19A produced using the wild-type *cry19A* operon (pJEG65.5) in *B. thuringiensis* 4Q7; lane 2, Cry19A synthesized using the *cry19A* operon under the control of *cyt1A*-p/STAB-SD (pSTAB-19Aopn) in *B. thuringiensis* 4Q7.

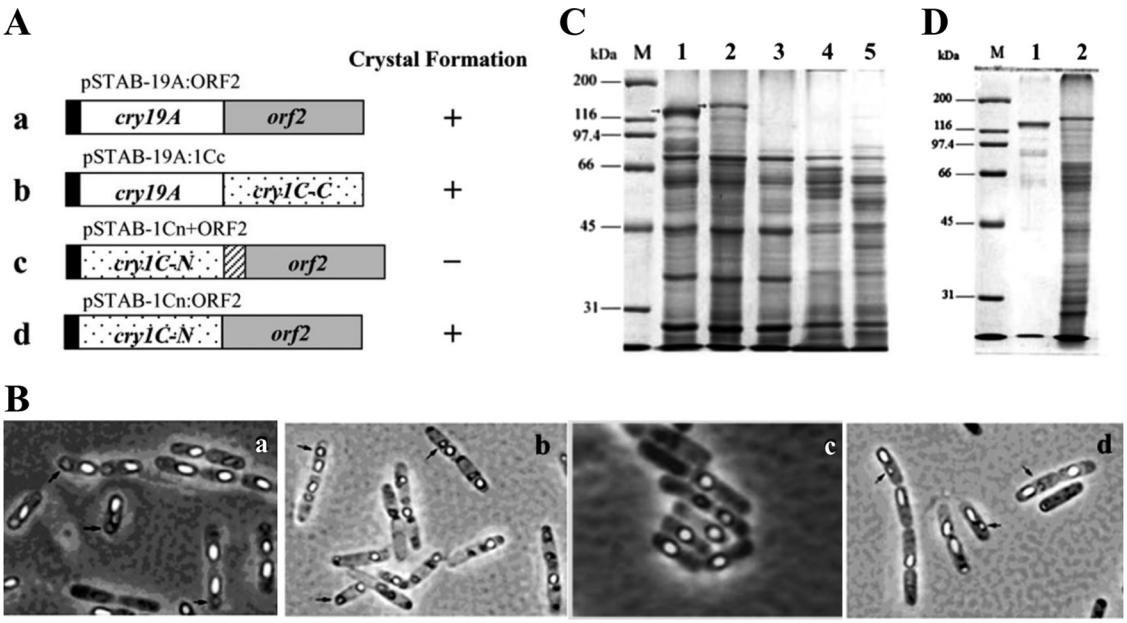

FIG 3 Functional analysis of ORF2. (A) Schematic illustration of the different constructs used to synthesize Cry19A and test the function of the 60-kDa ORF2 protein. In all constructs, expression was under the control of the *cyt1A*-p/STAB-SD sequence. Strains that contained or lacked crystals are indicated by (+) or (−), respectively. Panel a, pSTAB-19A:ORF2 used to synthesize a chimeric Cry19A:ORF2 protein. For this construct, the *cry19A* stop codon and intergenic spacer sequence were removed. Panel b, pSTAB-19A:1Cc used to determine whether the C-terminal half of Cry1C could be used to assist crystallization of Cry19A. For this construct, the *cry19A* stop codon and intergenic spacer sequence were removed and ligated with the region coding for the C-terminal half of Cry1C. Panel c, pSTAB-1Cn+ORF2 operon used to synthesize N-terminal half of Cry1C and ORF2 together; this construct contained the coding region of the N-terminal half of Cry1C with an artificial stop codon and *orf2* that included the intergenic spacer naturally present in the *cry19A* operon. Panel d, pSTAB-1Cn:ORF2 used to synthesize a chimeric N-terminal half of Cry1C:ORF2. (B) Phase-contrast micrographs of the recombinant *B. thuringiensis* 4Q7 strains containing the plasmids illustrated in panel A. Arrows indicate crystals. Panel a, 4Q7/pSTAB-19A:ORF2; panel b, 4Q7/pSTAB-19A:1Cc; panel c, 4Q7/pSTAB-1Cn+ORF2; panel d, pSTAB-1Cn:ORF2. (C) SDS-PAGE analysis of spore-crystal mixtures of *B. thuringiensis* strains grown in NBG medium. Lane M, molecular mass markers; lane 1, *B. thuringiensis* 4Q7 transformed with pSTAB-19A:ORF2; lane 2, *B. thuringiensis* 4Q7 transformed with pSTAB-19A:1Cc; lane 3, *B. thuringiensis* 4Q7 transformed with the pSTAB-1Cn+ORF2 operon that included the intergenic spacer naturally present in the *cry19A* operon; lane 4, *B. thuringiensis* 4Q7 transformed with pSTAB-1Cn:ORF2 without the intergenic spacer; lane 5, *B. thuringiensis* 4Q7 transformed with pSTAB. Arrows indicate the chimeric proteins produced. (D) SDS-PAGE analysis of purified crystals. Lane M, molecular mass markers; lane 1, *B. thuringiensis* 4Q7 transformed with pSTAB-19A:ORF2; lane 2, *B. thuringiensis* 4Q7 transformed with pSTAB-19A:1Cc.

ligated with pSTAB as described previously (11). The sequence integrity of all plasmid constructs was confirmed by restriction enzyme digestion and nucleotide sequencing.

Transformation of *B. thuringiensis*. Competent cells for transformation were prepared as described by Park et al. (16). A cell suspension (300 μl) was mixed with 5 μg of the plasmid construct and held on ice for 10 min. Electroporation was performed with a 0.2-cm electroporation cuvette (VWR, Bristol, CT) in a BTX ECM630 pulser apparatus set at 2.3 kV, 475 Ω, and 25 μF. After the pulse, the electroporated mixture was added to 3 ml of brain heart infusion (BHI) (Beckton, Dickinson and Company, Sparks, MD) and incubated with gentle shaking (60 rpm) for 1 h at 37°C. Transformants were selected on BHI supplemented with 25 μg of erythromycin and/or 5 μg of chloramphenicol.

Protein analysis. Bacterial cultures were harvested after 3 days of growth in GYS (14) or NBG (14) medium with shaking at 250 rpm at 30°C. The pellets were resuspended in 5 ml of double-distilled water and sonicated three times for 60 s using a model 4710 ultrasonic homogenizer (Cole-Palmer Instrument Co., Chicago, IL). After centrifugation, the pellet was washed with double-distilled water and 0.5 M NaCl, resuspended in 150 μl of 5× Laemmli sample buffer (8), and boiled for 5 min. Replicate aliquots of 10 μl of samples were separated by sodium dodecyl sulfate-polyacrylamide gel electrophoresis (SDS-PAGE) in a 10% gel as described by Laemmli (8). Protein mass was estimated by comparison with the protein size marker (Bio-Rad, Hercules, CA). For crystal purification, 5 ml of sonicated samples was loaded on a discontinuous sucrose gradient (67%, 72%, and 79% [wt/vol]) and then centrifuged at 18,000 × *g* for 80 min at 4°C using a Beckman L7-55 ultracentrifuge (11). Bands containing inclusions were collected and dialyzed in double-distilled water overnight at 4°C. Protein concentration was determined by the Bradford method (13).

Amino acid sequence alignments. Homology searches with ORF2 (GenBank accession number Y07603) were performed using the Basic Local Alignment Search Tool (BLAST) (BLASTP version 2.2.2; http://www.ncbi.nlm.nih.gov/). ORF2 and Cry protein sequences that showed the highest level of identity were then aligned using Vector NTI software (Carlsbad, CA).

Microscopy. Sporulating cultures were monitored with a Zeiss Photomicroscope III instrument. For scanning electron microscopy, crystals were separated from spores by sucrose density gradient centrifugation as described above, washed three times with double-distilled water, and dialyzed in double-distilled water (13, 14). Crystals in aqueous suspensions were placed on stubs, examined, and photographed using a Phillips XL30 scanning electron microscope.

Bioassays. Lyophilized cultures containing spores and crystals were suspended in double-distilled water. Suspensions were diluted to 6 or 7 different concentrations in 6-oz cups in a final volume of 100 ml. Bioassays were replicated three times using 30 4th instars of *Culex quinquefasciatus* (S-Lab strain; courtesy of M. C. Wirth, Department of Entomology, University of California, Riverside, CA) per concentration. After 48 h of exposure at 28°C, dead larvae were counted and the median (50%) lethal concentration (LC_{50}) and LC_{95} were calculated by Probit analysis (POLO-PC; LeOra Software, Berkeley, CA).

RESULTS

ORF2 is required for crystallization of Cry19A. When sporulated cells were examined by phase-contrast microscopy, crystalline inclusions were produced only when both *cry19A* and *orf2* were present in the constructs, whether in *cis* or *trans* (Fig. 1A). More specifically, sporulated cells (>99%) of *B. thuringiensis* 4Q7 containing the entire native *cry19A* operon (4Q7/pJEG65.5) produced spherical to oval crystals as large as the accompanying spores (Fig. 1B, panel 1), whereas *B. thuringiensis* 4Q7 strains containing the entire operon with point mutations in the translation codon of *cry19A* or *orf2* (4Q7/pHTΔ19ORF2 or 4Q7/pHT19ΔORF2, respectively) or the intact *cry19A* or *orf2* alone (4Q7/pPG19 or 4Q7/pHTORF2, respectively) did not produce visible inclusions during sporulation (Fig. 1B, panels 2 to 5). In contrast, when plasmids containing *cry19A* (pPG19) and *orf2* (pHTORF2) were introduced separately in different expression vectors yielding the recombinant strain 4Q7/pPG19+pHTORF2, inclusions were observed that were similar in morphology and size to those produced in strain 4Q7 harboring the wild-type operon (pJEG65.5) (Fig. 1B, panel 6).

To determine whether a detectable level of insoluble Cry19A accumulated in recombinants lacking visible inclusions, as determined by microscopy, equal amounts of GYS culture medium containing the different strains were analyzed by SDS-PAGE (Fig. 1C). The protein profile of the 4Q7/pJEG65.5 control strain showed that it produced the highest level of Cry19A (Fig. 1C, lane 1), which was consistent with phase-contrast microscopy showing larger crystalline inclusions in this strain. Strain 4Q7/pPG19+pHTORF2, which produced a smaller Cry19A crystal than 4Q7/pJEG65.5, also showed the presence of Cry19A, and the relative unit yield per volume was significantly less than that of 4Q7/pJEG65.5 (Fig. 1C, lane 6). The protein profiles of the acrystalliferous recombinant strains, i.e., 4Q7/pHTΔ19ORF2, 4Q7/pHT19ΔORF2, 4Q7/pPG19, and 4Q7/pHTORF2, lacked a distinct band corresponding to Cry19A (Fig. 1C, lanes 2 to 5).

Overexpression of the *cry19A* operon stabilizes the bipyramidal morphology of Cry19A crystalline inclusions. Microscopy of replicate cultures of 4Q7/pJEG65 suggested that pleomorphic crystals (spherical, cuboidal, and bipyramidal) were synthesized during sporulation. To determine whether Cry19A crystals of uniform size and shape could result from overexpression of the operon, the *cry19A* (pSTAB-19A) or *cry19A* and *orf2* (pSTAB-19Aopn) coding sequences were expressed using the strong chimeric *cyt1A*-p/STAB-SD expression system (12) (Fig. 2A). No inclusions were observed in 4Q7/pSTAB-19A that lacked ORF2, whereas crystals of apparently uniform shape and size were seen in 4Q7/pSTAB-19Aopn (Fig. 2B). The presumed differences in crystalline morphology were confirmed by electron microscopy (Fig. 2C). Micrographs of Cry19A inclusions produced by 4Q7/pJEG65.5 showed variations in shape, with most appearing to be cuboidal and to a lesser extent bipyramidal or a combination of these shapes (Fig. 2C, panel a). The cuboidal inclusions averaged 0.47 μm in length by 0.32 μm in width (Fig. 2C, panel a; Table 3). These results were observed in replicate culture preparations to rule out cross-contamination with other laboratory strains of *B. thuringiensis*. Crystals produced by 4Q7/pSTAB-19Aopn were significantly larger, averaging 1.1 μm in length by 0.61 μm in width, and had a uniform shape similar to that of the classic bipyramidal crystals formed by 135-kDa Cry proteins (Fig. 2C, panel b; Table 3). Using these dimensions to calculate the approximate crystal volumes, crystals resulting from overexpression of the recombinant operon were approximately 4-fold larger than those produced in the strain harboring the wild-type operon.

TABLE 3 Dimensions of Cry19A crystals produced by two recombinant strains of *Bacillus thuringiensis*[a]

Strain	Toxin combination	Crystal length (μm)	Crystal width (μm)
4Q7/pJEG65.5	Cry19A + ORF2	0.47 ± 0.06 a	0.32 ± 0.07 a
4Q7/pSTAB-19Aopn	Cry19A + ORF2	1.10 ± 0.11 b	0.61 ± 0.06 b

[a] Means for each crystal dimension were calculated from measurements ($n = 10$) determined using scanning electron micrographs. Values followed by different letters were significantly different at $P = 0.05$.

SDS-PAGE analysis showed that the amount of Cry19A synthesized by 4Q7/pSTAB-19Aopn was 5.5-fold greater than that produced by 4Q7/pJEG65.5, which harbored the wild-type *cry19A*, and little or no Cry19A was detected in 4Q7/pSTAB-19A that lacked *orf2* (Fig. 2D, panel a). When similar quantities of purified, solubilized Cry19A crystals produced using either *cyt1A*-p/STAB-SD or the wild-type promoter to express the *cry19A* operon were analyzed by SDS-PAGE, the three proteins previously reported, one of 65 kDa corresponding to Cry19A and two of 66 and 67 kDa corresponding to ORF2 (19), were found in both preparations (Fig. 2D, panel b).

ORF2 functions as a C-terminal domain for crystallization of Cry19A. The results presented above indicated that the presence of *orf2* in *cis* is not essential for subsequent synthesis and crystallization of Cry19A; i.e., it is unlikely that the *orf2* sequence functioned as an mRNA stabilizer. Therefore, ORF2 could potentially function as a molecular chaperone or a C-terminal domain for aggregation of Cry19A, as it was required for crystal assembly. To test the latter hypothesis, we constructed four recombinant plasmids containing combinations of *cry19A* and *orf2* or the cry1C N terminus (Cry1C-N) and *orf2* in frame or separated by the wild-type intergenic spacer (Fig. 3A). In addition, the strong *cyt1A*-p/STAB-SD (12) promoter was used for expression of these constructs because we observed that crystals obtained using the wild-type promoter were not uniform in shape and size whereas those resulting from expression with *cyt1A*-p/STAB-SD were uniformly bipyramidal (Fig. 2C). Plasmid pSTAB-19A:ORF2 contained *cry19A* in frame with *orf2*; pSTAB-19A:1Cc contained *cry19A* in frame with the C-terminal half of Cry1C; pSTAB-1Cn+ORF2 contained the fragment encoding the N-terminal half of Cry1C with a stop codon, the intergenic spacer sequence of *cry19A* operon, and *orf2*; and pSTAB-1Cn:ORF2 contained the fragment encoding the N-terminal half of Cry1C in frame with *orf2*.

Microscopy of sporulated cells (Fig. 3B) showed that 4Q7/pSTAB-19A:ORF2 (panel a) produced bipyramidal crystals, whereas 4Q7/pSTAB-19A1Cc (panel b) produced inclusions with various shapes such as those observed in 4Q7/pJEG65.5. Visible crystalline inclusions were not detected in 4Q7/pSTAB-1Cn+ORF2 (panel c), whereas inclusion bodies that were relatively much smaller were observed in 4Q7/pSTAB-1Cn:ORF2 (panel d). SDS-PAGE profiles of sporulated cultures (Fig. 3C) showed the presence of the predicted chimeric crystalline proteins in 4Q7/pSTAB-19A:ORF2 (Cry19A:ORF2; 135 kDa) and 4Q7/pSTAB-19A:1Cc (Cry19A:1Cc; 138 kDa). Unique bands corresponding to Cry1C N terminus (68 kDa; 4Q7/pSTAB-

1Cn+ORF2) or Cry1Cn:ORF2 (128 kDa; 4Q7/pSTAB-1Cn:ORF2) were not apparent in SDS-PAGE (Fig. 3C). The latter observation suggested that the smaller inclusions in 4Q7/pSTAB-1Cn:ORF2 were unstable.

To confirm that the novel bands observed in the protein profiles of the recombinant strains represented chimeric proteins, inclusions were purified on discontinuous sucrose gradients and analyzed by SDS-PAGE (Fig. 3D). This analysis confirmed the presence of Cry19A:ORF2 (135 kDa) and Cry19A:1Cc (138 kDa) chimeric proteins. Inclusions of Cry1CnORF2 were not recovered in sucrose gradients, suggesting that they were unstable under the parameters used in this study.

Sequence analysis. The amino acid sequence alignment showed that ORF2 shared the highest level of identity with the C-terminal region of Cry4Aa (66%), Cry4Ba (66%), Cry8Aa (47%), Cry28Aa (46%), Cry7Ab (44%), Cry9Da (41%), and Cry26Aa (41%) (Fig. 4). Amino acid residues from 156 to 209 of ORF2 showed the least identity with C termini of other Cry proteins.

Bioassays. The toxicity of wild-type and recombinant strains of *B. thuringiensis* was evaluated against 4th instars of *C. quinquefasciatus* (Table 4). Strain 4Q7/pSTAB-19A, which produced the smallest and apparently unstable inclusions, was not toxic at 10 μg/ml. Strains 4Q7/pJEG65.5 and 4Q7/pSTAB-19Aopn showed moderate toxicity, with no significant differences in their median lethal concentrations (LC_{50}s). However, according to the LC_{95} values, the 4Q7/pSTAB-19Aopn strain was approximately 4-fold more toxic (1.9 μg/ml) than 4Q7/pJEG65.5 (8.2 μg/ml), the strain containing the wild-type operon. Interestingly, 4Q7/pSTAB-19A:ORF2, which produced stable inclusions of the Cry19A:ORF2 fusion protein, showed poor toxicity, even at 10 μg/ml, and the other two strains that produced, respectively, the chimeric protein of Cry19A and C terminus of Cry1C (pSTAB-19A:1Cc) and the chimeric protein of N terminus of Cry1C and ORF2 (pSTAB-1Cn:ORF2) showed no toxicity at a concentration of 10 μg/ml (data not shown).

DISCUSSION

The initial report by Rosso and Delécluse (19) suggested that *orf2* of the *Cry19A* operon could potentially function as a *cry19A* mRNA-stabilizing sequence or that the coded 60-kDa ORF2 protein could function as a molecular chaperone for crystallization of Cry19A. However, insufficient data were presented in that study to determine the role of ORF2, especially as one of the crystalliferous deletion mutants used in the analysis retained only ~75% of the 5′ region of *orf2*. Our results demonstrating that stable crystalline inclusions accrue in strains that harbor *cry19A* and *orf2*, expressed either in *cis* or *trans*, provide strong evidence that ORF2 functions primarily as a C-terminal crystallization domain, as is known for large Cry proteins. The evidence for this is that (i) the two proteins appear in approximately equimolar amounts when observed by acrylamide gel electrophoresis, a phenomenon unlikely to occur with typical chaperonins (20); (ii) the fusion Cry19A:ORF2 protein forms stable crystals; (iii) when fused in frame with the N-terminal region of Cry1C, the chimeric protein (Cry1Cn:ORF2) forms visible inclusions, even though these are unstable, in sporulating cells of strain 4Q7 (Fig. 3); and (iv) ORF2 shares a considerable level of identity with the C-terminal region of large Cry proteins (Fig. 4). In addition, the observation that Cry19A crystallizes when fused in frame with the C-terminal region of Cry1C (Cry19A:1Cc) demonstrates the necessity of a C-terminal domain, a function provided by ORF2 (Fig. 3). We do not have a clear explanation why the N-terminal region of Cry1C did not crystallize in the presence of ORF2, but it possible that sequences that mediate intermolecular interactions between the two proteins are lacking or that the chimeric protein in the absence of appropriate stabilizing peptides is degraded by intrinsic proteases.

Most Cry proteins have a mass in the range of 130 to 135 kDa and typically do not require other proteins for synthesis and crystallization. Thus, genes that encode these occur alone rather than in operons. However, several *cry* genes coding for proteins in the 65-kDa range occur in operons in which the proteins encoded by the other genes affect net synthesis and crystallization. For example, the 20-kDa protein encoded by *orf3* in the *cry11Aa* operon increases Cry11Aa synthesis by 2-fold, possibly acting as a molecular chaperone (27, 28), whereas the 29-kDa protein encoded by *cry2Aa* operon *orf2* apparently forms a matrix that facilitates formation of the "cushion-shaped" Cry2Aa inclusion (6). Interestingly, Cry19A contains the five conserved blocks present in the N-terminal half of most Cry proteins, for example, Cry1, Cry4, Cry7, and Cry8 (21). Thus, Cry19A (75 kDa) and its associated ORF2 protein (60 kDa) together have features similar to those of 135-kDa Cry proteins. Therefore, it is tempting to speculate that mutations accrued in the extant intergenic region (149 bp) between *cry19A* and *orf2* that resulted in a two-gene operon. However, successive mutations would be required if such were the case, as the intergenic region contains five stop codons in frame with *orf19A*, a single frameshift proximal to the start codon of *orf2*, and a canonical Shine-Dalgarno (ribosome binding site) sequence for efficient translation of *orf2*, as observed in the sequence reported by Rosso and Delécluse (19).

The appearance of large uniformly bipyramidal Cry19A crystals resulting from overexpression of the operon suggests that stable crystal morphology is directly linked to the concentration of the larvicidal toxin that accumulates in the cell during sporulation. Definitive data have not been reported on the relative activity of the wild-type promoter during vegetative or the sporulation phases of growth or on the stability of the *cry19A/orf2* transcript. In contrast, it is known that multiple promoters and an mRNA-stabilizing sequence are present in *cyt1A*-p/STAB-SD (12), factors that result in overexpression and stability of the transcript and subsequent increased levels of Cry19A and ORF2 synthesis during sporulation.

With respect to *cry* operons, only three (*cry10Aa*, *cry39Aa*, and *cry40Aa*) have a gene organization similar to that of the *cry19A* operon (3). Their upstream reading frames code for the Cry N-terminal domain, and the second frame found approximately 100 bp downstream (3) codes for an apparent C-terminal domain that presumably has a function similar to that of ORF2 in protoxin aggregation and crystallization.

Finally, with regard to Cry19A's applied potential, the statistically significant increase in toxicity at the LC_{95} level observed with the recombinant strain that expressed the *cry19A* operon by the use of *cyt1A*-p/STAB-SD (4Q7/pSTAB-19Aopn) in comparison to the toxicity of the strain that expressed the wild-type operon (SPL407/pJEG 65.5) demonstrates the versatility of the strong *cyt1A*-p/STAB-SD expression system. Indeed, the increase in toxicity is likely due to larger Cry19A crystals and the increased yield of Cry19A produced per unit of medium using the recombinant

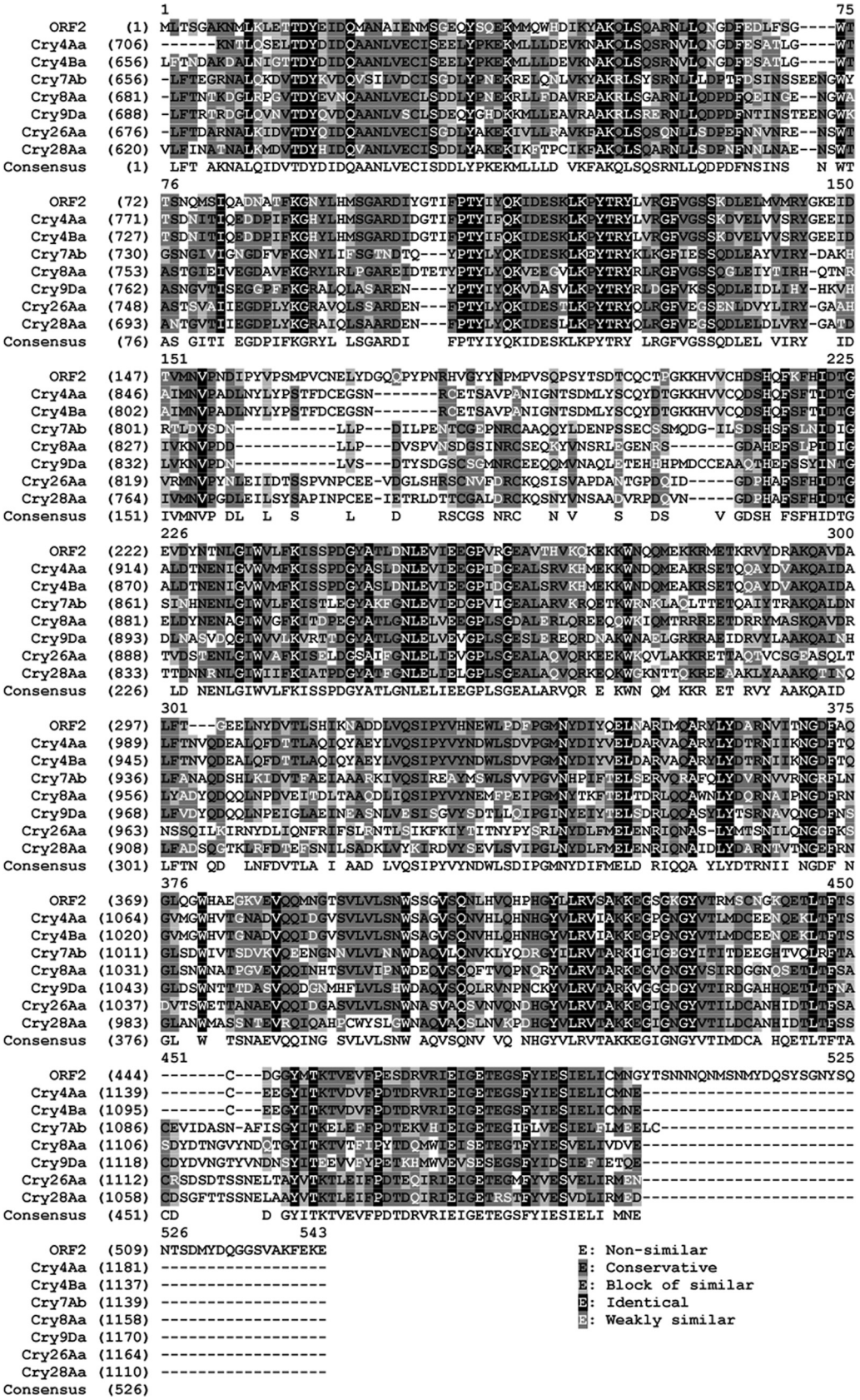

FIG 4 Alignment of the ORF2 amino acid sequence with C-terminal regions of selected Cry proteins.

TABLE 4 Toxicity of parental and recombinant strains of *Bacillus thuringiensis* to *Culex quinquefasciatus*

Strain	Toxin combination	LC_{50}[a]	LC_{95}[a]	Slope
4Q7/pJEG 65.5	Cry19A + ORF2	0.6 (0.4–0.9)	8.2 (4.0–29.5)	1.5 ± 0.2
4Q7/pSTAB-19A	Cry19A	Nt[b]	Nt	Nt
4Q7/pSTAB-19Aopn	Cry19A + ORF2	0.4 (0.3–0.6)	1.9 (1.3–3.6)	2.6 ± 0.4

[a] Values are shown in micrograms of spore-crystal mixture per milliliter and represent 48-h mortality determined by Probit analysis. Confidence limits are indicated in parentheses.
[b] Nt, not toxic at 10 μg/ml.

promoter. The improved activity observed only at LC_{95} indicates that Cry19A may be solubilized or activated more slowly in target mosquito species than other mosquitocidal Cry proteins. At present, whether the enhanced Cry19A has increased toxicity to other mosquito species is unknown. Further studies are required to demonstrate the efficacy of the larger protoxin inclusions alone or in combination with other mosquitocidal toxins against mosquito species of medical importance.

ACKNOWLEDGMENTS

We thank Jeffrey J. Johnson for technical assistance during this study.

This research was supported by a sabbatical leave funding and a grant from the University of California MEXUS-CONACYT program (CN02-106) to J.E.B.-C., a grant from the United States Department of Agriculture (CSREES 2007-38814-18497) to H.-W.P., and grants from the U.S. Department of Agriculture (CSREES 2001-35302-09974) and National Institutes of Health (1 RO1 AI45817) to B.A.F.

REFERENCES

1. **Berry C, et al.** 2002. Complete sequence and organization of pBtoxis, the toxin-coding plasmid of *Bacillus thuringiensis* subsp. *israelensis*. Appl. Environ. Microbiol. **68**:5082–5095.
2. **Delécluse A, Rosso ML, Ragni A.** 1995. Cloning and expression of a novel toxin gene from *Bacillus thuringiensis* subsp. *jegathesan* encoding a highly mosquitocidal protein. Appl. Environ. Microbiol. **61**:4230–4235.
3. **de Maagd RA, Bravo A, Berry C, Crickmore N, Schnepf HE.** 2003. Structure, diversity, and evolution of protein toxins from spore-forming entomopathogenic bacteria. Annu. Rev. Genet. **37**:409–433.
4. **Federici BA, Park H-W, Bideshi DK.** 2010. Overview of the basic biology of *Bacillus thuringiensis* with emphasis on genetic engineering of bacterial larvicides for mosquito control. Open Toxinol. J. **3**:154–171.
5. **Federici BA, Park H-W, Sakano Y.** 2006. Insecticidal protein crystals of *Bacillus thuringiensis*, p 195–236. *In* Shively JM (ed), Microbiology monographs, vol 1: inclusions in prokaryotes. Springer-Verlag, Heidelberg, Germany.
6. **Ge B, Bideshi D, Moar WJ, Federici BA.** 1998. Differential effects of helper proteins encoded by the *cry2A* and *cry11A* operons on the formation of Cry2A inclusions in *Bacillus thuringiensis*. FEMS Microbiol. Lett. **165**:35–41.
7. **Georghiou G, Wirth MC.** 1997. Influence of exposure to single versus multiple toxins of *Bacillus thuringiensis* subsp. *israelensis* on development of resistance in the mosquito *Culex quinquefasciatus* (Diptera: Culicidae). Appl. Environ. Microbiol. **63**:1095–1101.
8. **Laemmli UK.** 1970. Cleavage of structural proteins during the assembly of the head bacteriophage T4. Nature **227**:680–685.
9. **Lereclus D, Arantes O, Chaufaux J, Lecadet M.** 1989. Transformation and expression of a cloned delta-endotoxin gene in *Bacillus thuringiensis*. FEMS Microbiol. Lett. **51**:211–217.
10. **Park HW, Delécluse A, Federici BA.** 2001. Construction and characterization of a recombinant *Bacillus thuringiensis* subsp. *israelensis* strain that produces Cry11B. J. Invertebr. Pathol. **78**:37–44.
11. **Park HW, Federici BA.** 2000. Domain I plays an important role in the crystallization of Cry3A in *Bacillus thuringiensis*. Mol. Biotechnol. **16**:97–108.
12. **Park HW, Ge B, Bauer LS, Federici BA.** 1998. Optimization of Cry3A yields in *Bacillus thuringiensis* by use of sporulation-dependent promoter in combination with the STAB-SD mRNA sequence. Appl. Environ. Microbiol. **64**:3932–3938.
13. **Park HW, Bideshi DK, Federici BA.** 2000. Molecular genetic manipulation of truncated Cry1C protein synthesis in *Bacillus thuringiensis* to improve stability and yield. Appl. Environ. Microbiol. **66**:4449–4455.
14. **Park HW, Bideshi DK, Johnson JJ, Federici BA.** 1999. Differential enhancement of Cry2A versus Cry11A yields in *Bacillus thuringiensis* by use of the *cry3A* STAB mRNA sequence. FEMS Microbiol. Lett. **181**:319–327.
15. Reference deleted.
16. **Park H-W, et al.** 2005. Recombinant larvicidal bacteria with markedly improved efficacy against *Culex* vectors of West Nile virus. Am. J. Trop. Med. Hyg. **72**:732–738.
17. **Ragni A, Thiéry I, Delécluse A.** 1996. Characterization of six highly mosquitocidal *Bacillus thuringiensis* strains that do not belong to H-14 serotype. Curr. Microbiol. **32**:48–54.
18. Reference deleted.
19. **Rosso ML, Delécluse A.** 1997. Contribution of the 65-kilodalton protein encoded by the cloned gene *cry19A* to the mosquitocidal activity of *Bacillus thuringiensis* subsp. *jegathesan*. Appl. Environ. Microbiol. **63**:4449–4455.
20. **Sabate R, de Groot NS, Ventura S.** 2010. Protein folding and aggregation in bacteria. Cell. Mol. Life Sci. **67**:2695–2715.
21. **Schnepf E, et al.** 1998. *Bacillus thuringiensis* and its pesticidal crystal proteins. Microbiol. Mol. Biol. Rev. **62**:775–806.
22. **Seleena P, Lee HL, Lecadet MM.** 1995. A new serovar of *Bacillus thuringiensis* possessing 28a28c flagellar antigenic structure: *Bacillus thuringiensis* serovar *jegathesan*, selectively toxic against mosquito larvae. J. Am. Mosq. Control Assoc. **11**:471–473.
23. Reference deleted.
24. **Wirth MC, Delécluse A, Walton WE.** 2001. Lack of cross-resistance to Cry19A from *Bacillus thuringiensis* subsp. *jegathesan* in *Culex quinquefasciatus* (Diptera: Culicidae) resistant to Cry toxins from *Bacillus thuringiensis* subsp. *israelensis*. Appl. Environ. Microbiol. **67**:1956–1958.
25. **Wirth MC, Delécluse A, Federici BA, Walton WE.** 1998. Variable cross-resistance to Cry11B from *Bacillus thuringiensis* subsp. *jegathesan* in *Culex quinquefasciatus* (Diptera: Culicidae) resistant to single or multiple toxins of *Bacillus thuringiensis* subsp. *israelensis*. Appl. Environ. Microbiol. **64**:4174–4179.
26. **Wirth MC, Georghiou GP, Federici BA.** 1997. CytA enables CryIV endotoxins of *Bacillus thuringiensis* to overcome high levels of CryIV resistance in the mosquito, *Culex quinquefasciatus*. Proc. Natl. Acad. Sci. U. S. A. **94**:10536–10540.
27. **Wu D, Federici BA.** 1993. A 20-kilodalton protein preserves cell viability and promoters CytA crystal formation during sporulation in *Bacillus thuringiensis*. J. Bacteriol. **175**:5276–5280.
28. **Wu D, Federici BA.** 1995. Improved production of the insecticidal CryIVD protein in *Bacillus thuringiensis* using *cryIA*(*c*) promoter to express the gene for an associated 20-kDa protein. Appl. Microbiol. Biotechnol. **42**:697–702.
29. Reference deleted.